Marquette University

e-Publications@Marquette

Electrical and Computer Engineering Faculty Research and Publications

Electrical and Computer Engineering, Department of

9-2015

Error Probabilities for Optical Receivers That Employ Dynamically Biased Avalanche Photodiodes

Georges El-Howayek

Majeed M. Hayat

Error Probabilities for Optical Receivers That Employ Dynamically Biased Avalanche Photodiodes

Georges El-Howayek
Department of Electrical and Computer Engineering, University of New Mexico, Albuquerque, NM
Majeed M. Hayat
Department of Electrical and Computer Engineering, University of New Mexico, Albuquerque, NM

Abstract

A novel theory was recently reported for the avalanche multiplication process in avalanche photodiodes (APDs) under dynamic reverse-biasing conditions. It has been shown theoretically that the bit-synchronized, periodic modulation of the electric field in the multiplication region can offer improvements in the gain-bandwidth product by reducing intersymbol interference in optical receivers. This paper reports a rigorous formulation of the sensitivity of optical receivers that employ dynamically biased APDs. To enable the sensitivity analysis, a

recurrence theory is developed to calculate the joint probability distribution function (PDF) of the stochastic gain and avalanche buildup time in APDs that are operated under dynamic biasing. It is shown that in an ideal buildup-time limited scenario, a minimum receiver sensitivity of -20 dBm is predicted at an optimal gain of approximately 47 for a 60 Gb/s communication system, compared to a minimum of 0 dBm in the static-bias case. The receiver sensitivity analysis also reveals that, as the peak-to-peak voltage of the dynamic reverse bias increases, the device optimal gain increases while maintaining a short avalanche buildup time and reduced ISI. Of course, a point of diminishing return exists in practice when the tunneling current in the multiplication region becomes dominant.

SECTION I. Introduction

To meet the demands of the exponential growth in video, voice, data and mobile device traffic over the internet, the telecommunication industry has been moving toward higher-speed protocols [1]. The Synchronous Optical Network standards, OC-48 and OC-192, specify the data rates in optical networks as 2.5 Gb/s [2] and 10 Gb/s [3], respectively; however, the data rates are increasing to 40 Gb/s and 100 Gb/s [4] for more recent standards. InGaAs pin diodes have been the preferred choice in high speed optical communications due to their good electron transport properties and their low loss absorption in the 1.0–1.7 µm wavelength region [5]. Several proposed structures for pin diodes meet the requirements of the OC-192 and the OC-768 standards [6], [7]. Presently, the only commercially viable option for direct detection in 40-Gb/s long-haul optical links is the InGaAs pin photodiode combined with optical preamplification, since very high bandwidth and sensitivity can be achieved with this combination [8]. However, these receivers can be bulky and expensive due to their optical-amplifier requirement. The need for optical pre-amplification may be removed by using an avalanche photodiodes (APDs), in which an internal gain is generated by converting each detected photon into a cascade of offspring electrons and holes. It is well known that the internal gain of APDs provides a higher sensitivity in optical receivers than that of pin photodiodes [9]– [10] [11] [12].

Although APDs have been successfully deployed in 10 Gb/s optical communication systems [13], [14], moving their utility to higher speeds has been a big challenge due to the avalanche buildup time, which is the stochastic time required for the cascade of impact ionizations to complete each time an avalanche is triggered. The avalanche buildup time limits the receiver performance by inducing intersymbol interference (ISI) at high speeds [15]– [16] [17]. Numerous attempts have been recorded to achieve higher data rates through the use of APDs with separate absorption and multiplication layers; these include APDs with thin multiplication regions [18], [19] as well as impact-ionization engineering of the multiplication region [20]. Recently, Hayat and Ramiraz[21], [22] proposed a novel approach for operating APDs in the linear mode while employing bit-synchronous and sinusoidal dynamic biasing that can reduce the buildup time dramatically in any buildup-time limited APD-based optical receiver. The essence of the dynamic-biasing approach is to promote very strong impact ionizations in the early phase of an optical bit (to benefit from the high gain) while suppressing the ionizations near the end of the bit (to reduce ISI). They showed that dynamic biasing can offer up to a five-fold increase in the gain-bandwidth product of the receiver when the dynamic bias is properly selected [23]. However, no analysis of the receiver sensitivity has been developed to date for dynamically biased APDs. The requirement that the dynamic biasing of the APD should be synchronous with the data stream can be implemented easily in practice. The approach would be to use the output of the clock/data recovery (CDR) circuit, which is standard in any optical receiver, and use it as the input to a sine-wave generator, which makes it synchronous to the data stream.

In this paper, we rigorously analyze the APD's sensitivity under dynamic biasing. To enable the calculation of the bit-error rate (BER) under an on-off keying (OOK) setting, we develop the first theory for the joint probability distribution of the stochastic gain and stochastic buildup time in dynamically biased APDs. This development

constitutes a major expansion of (i) the recursive equations developed in [15] under the traditional assumption of a static bias, and (ii) the recursive technique characterizing the gain and buildup time individually [21]. The new theory enables us to calculate the statistical properties of the APD's photocurrent, such as its mean, variance and autocorrelation function all under dynamic biasing. This, in turn, is used to formulate analytically the sensitivity of a dynamically biased APD-based receiver and to optimize the sensitivity over system and device parameters. The analysis in this paper will specifically capture the effects of ISI and dark current, as well as transimpedance-amplifier noise (used in the pre-amplification stage of receivers). The sensitivity formulation developed here can be used as a guide in designing dynamically biased APD-based receivers for specific system performance requirements well beyond the limits previously known under the traditional constant-bias setting.

The remainder of this paper is organized as follows. In Section II we present a recursive method to calculate the joint distribution of the gain and buildup-time of a dynamically biased APD. Numerical calculations for the joint statistics of the stochastic gain and stochastic buildup time are presented in Section III. In Section IV we approximate the impulse response function of the dynamically biased APD using a parametric model while exploiting the calculated joint statistics of stochastic gain and buildup time. Analytical expressions for the statistics of the output of the dynamically biased APD receiver are presented in Section V. Predictions of the receiver sensitivity are presented in Section VI, and the conclusions are drawn in Section VII.

SECTION II. Age-Dependent Recursive Theory for Joint Probability Distribution of Gain and Buildup Time Under Dynamic Biasing

For its relevance to this paper, we first begin by reviewing the proposed model introduced by Hayat and Ramirez in [21], which employs the use of a bit-synchronous and periodic dynamic biasing of an APD for linear-mode operation in direct-detection optical receivers. Next, we introduce the parameters and random variables required to derive the recursive equations that describe the joint probability distribution of gain and buildup time under dynamic biasing scheme.
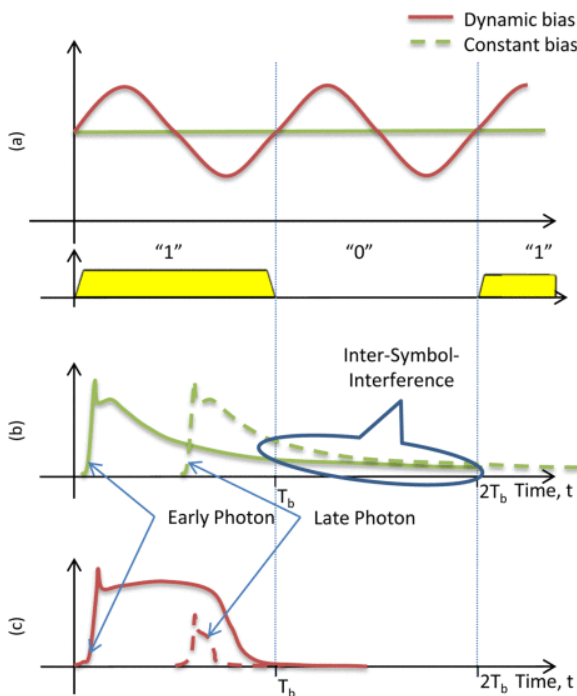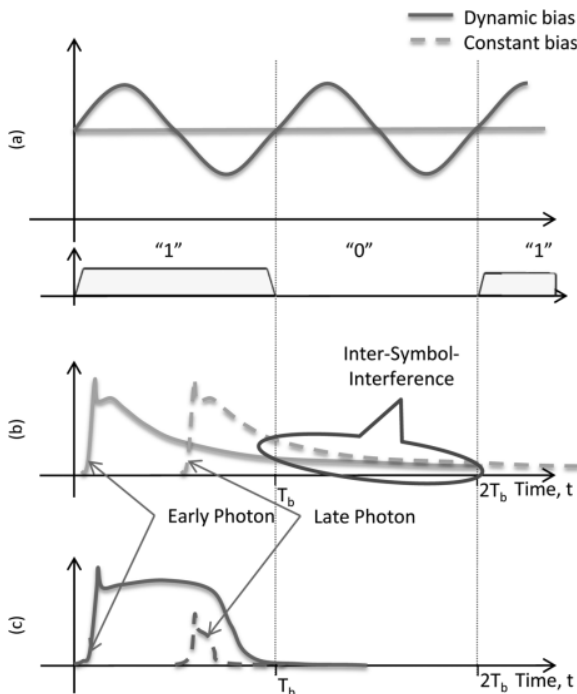
Fig. 1. The dynamic-biasing approach (red curves) reported in [21] compared with the traditional static-biasing approach (green curve). The impulse response of early photons has high avalanche gain but limited avalanche duration, and late photons trigger avalanches with low-gain and limited transit-time duration due to experiencing a weakened electric field in the multiplication region.

A. Review of the Dynamic-Biasing Approach

It was shown theoretically that the use of a bit-synchronous and periodic dynamic biasing of an APD can offer substantial reduction in the duration of the APD's pulse response, thereby minimizing ISI without sacrificing avalanche gain [21]. Specifically, a dynamic-biasing approach, with the same frequency of the pulse transmission rate as illustrated in Fig. 1 (red curve, top plot), can yield a pulse response with the following two properties. First, photons that arrive early in the optical pulse experience a period of high electric field in the multiplication region of the APD, where they can generate a strong avalanche current in the early phase of the optical-pulse window, as shown inFig. 1 (solid red curve, bottom plot). As a low electric field period follows the high-field phase within the optical pulse window, carriers in the multiplication region undergo a much weakened impact ionization process, which can lead to the termination (with high probability) of the stochastic avalanche current. Second, photons that arrive late in the optical-pulse window generate impulse responses that are characterized by a much reduced buildup time due to the weakening of impact ionization in the second phase of the bias period, as depicted schematically by the dashed red curve in Fig. 1. In contrast to traditional APD biasing which is static, the pulse response of the dynamically biased APD will be characterized by a high gain yet with a buildup time that is potentially terminated just before the start of the next bit. It was shown theoretically in [21] that the dynamic-biasing approach can improve the gain-bandwidth product (GBP) by a factor of 5 compared to the conventional static bias case. For instance, in an InP-based APD with a 200 nm multiplication width, the calculated gain-bandwidth product of the pulse response due to a 16.5-ps rectangular optical pulse was enhanced from 238 GHz in the static-bias case to a pulse gain-bandwidth product of 1169 GHz in the dynamic-bias case [21].

Following [21], the dynamic-field scenario brings about a new element to the analysis of impact ionization. This element is the age (or time stamp) of a carrier measured from the point in time when the dynamic bias is launched. The age will play a key role in the statistical analysis of the avalanche multiplication process. Specifically, carriers born at different times will experience different dynamical electric fields ahead of them as

they generate their own chains of impact ionizations. To take the age-factor into account in the analysis of the avalanche multiplication process, the usual ionization probability of a carrier is parameterized by the time at which the parent carrier is injected in the multiplication region. The key enabling idea in modeling the joint distribution for a dynamic reversed bias APD is to consider the age of the parent carrier relative to the launch instant of the dynamic bias as discussed next.

B. Definitions

Consider a multiplication region of the APD extending from $x = 0$ to $x = w$. Assume that a dynamic electric field, $E(t) = V(t)/w$, is present in the multiplication region, where $V(t)$ is the time-varying applied bias voltage. When a carrier enters the multiplication region at an age s relative to the launch of the dynamic bias, an age-dependent avalanche process will be triggered. For a parent carrier entering the multiplication region with age s and triggering an avalanche multiplication process, let T_s be the stochastic time required for the avalanche process to terminate, and let G_s be the total number of electron-hole pairs generated by this process. Note that T_s is the stochastic duration of the APD's impulse-response function induced by an injected carrier in the multiplication region with age s. Meanwhile, G_s is proportional to the area under the stochastic impulse-response function.

The age-dependent joint probability distribution function (PDF) associated with G_s and T_s is the probability that a parent carrier entering the multiplication region at age sgenerates m electron-hole pairs in a time less than or equal to t. Formally, we define the joint PDF as $f_{G_s,T_s}(m, t; s) = \text{P}\{G_s = m, T_s \leq t\}$. Following the concept of the recursive approach [21], let the random variable $Z(x, s)$ be the total number of electrons and holes (including the parent carrier) initiated by a parent electron located at location x with age s. Similarly, let $Y(x, s)$ be the total number of electrons and holes (including the parent carrier) initiated by a parent hole located at location x with age s. Note that if we assume that the electric field is in the opposite direction of the x-axis and the multiplication region span the region from $x = 0$ to $x = w$, by convention $Z(w, s) = Y(0, s) = 1, s \geq 0$, since an electron (hole) generated at the right (left) edge of the multiplication region will exit the multiplication region without ionization.

Let X_h and X_e be the stochastic free-path distances that the holes and electrons, respectively, travel before the impact ionization. The age-dependent probability density function of the free paths X_h and X_e, denoted by $h_h(\xi; x, s)$ and $h_e(\xi; x, s)$, respectively, were defined in [21] according to the dead-space multiplication theory (DSMT). Under a dynamic electric field, the probability density function of the first ionization by a parent carrier of age s and at location x is zero before the dead space is traveled and exponential with a nonuniform rate after the dead space. Specifically, in[21] these densities have been formulated as

$$h_h(\xi; x, s) = \begin{cases} \beta(\xi, s + \tau_h)e^{-\int_\xi^{x-d_h(x,s)} \beta(\sigma, s+\tau_h)d\sigma}, & \xi < x - d_h(x, s) \\ 0, & \text{otherwise} \end{cases}$$

and

$$h_e(\xi; x, s) = \begin{cases} \alpha(\xi, s + \tau_e)e^{-\int_{x+d_e(x,s)}^\xi \alpha(\sigma, s+\tau_e)d\sigma}, & \xi > x + d_e(x, s) \\ 0, & \text{otherwise} \end{cases}$$

where $\beta(x, t)$ and $\alpha(x, t)$ are the position and age dependent ionization coefficients, $d_h(x, s)$ and $d_e(x, s)$ represent the age-dependent dead spaces for a hole and electron, respectively, $\tau_e = (\xi - x)/v_e$ and $\tau_h = (x - \xi)/v_h$ is the electron and hole, respectively, transport time between x and ξ. Note

that $h_e(\xi; x, s)d\xi$ approximates the probability that an electron born at location x and of age s impact ionizes for the first time in the interval $[\xi, \xi + d\xi]$.

Other intermediate quantities required in this formulation are the buildup times. As in[21], define $Z(x, s)$ ($Y(x, s)$) as the totality of electrons and holes due to avalanche processes triggered by a parent electron (hole) of age s relative to the launch instant of the electric field. Now let $T_Z(x, s)$ be the random time required for the $Z(x, s)$ carries to exit the multiplication region; similarly, $T_Y(x, s)$ is defined in the same way. It is worth to mention that T_Z (or T_Y) is always greater than the electron (or hole) transport time between x and w, which is the time needed for the parent electron (or hole) to exit the multiplication region. We define the joint PDFs of the pairs (Z, T_Z) and (Y, T_Y) as follows:

$$
\begin{aligned}
f_e(m, t; x, s) &= P\{Z(x, s) = m, T_Z(x, s) \leq t\}, \\
f_h(m, t; x, s) &= P\{Y(x, s) = m, T_Y(x, s) \leq t\}.
\end{aligned} \quad \text{(1a)(1b)}
$$

Note that with this notation, the stochastic buildup time T_s defined earlier becomes $T_s = T_Y(w, s)$, and its corresponding stochastic gain is $G_s = 0.5(Y(w, s) + 1)$. For example, for an InGaAs-InP APD in which photo-generated holes are responsible for initiating avalanches in the InP multiplication region, we have $f_{G_s, T_s}(m, t, s) = f_h(2m - 1, t; w, s)$.

C. Recursive Equations

The key observation needed in the formulation of a recursion for the PDFs defined above is that a parent electron born at location x and of age s generates a certain number of offspring carriers ($Z(x, s) = m$, say) within a certain time ($T_Z(x, s) \leq t$, say) precisely when its two offspring electrons and offspring hole, born for example at location ξ, will collectively create the same intended number of carriers (m) albeit within a reduced time $t - \tau_e$. The age of the two offspring electrons and hole at birth is $s + \tau_e$. With this regeneration concept in mind and by using the fact that all carries impact ionize independently of one another other, and by averaging over all the possible locations $\xi \in [x, w]$ of the first ionization of the parent electron (using the probability density function h_e), we obtain the following recursive equation:

$$
\begin{aligned}
f_e(m, t; x, s) = \quad & g_e(x, t, s)\delta_{m-1} \\
& + \int_x^w [f_e(m, t - \tau_e; \xi, s + \tau_e) * f_e(m, t - \tau_e; \xi, s + \tau_e) \quad \text{(2)} \\
& * f_h(m, t - \tau_e; \xi, s + \tau_e)]h_e(\xi; x, s)d\xi,
\end{aligned}
$$

where δ_i is the Kronecker delta function ($\delta_i = 1$ when $i = 0$ and zero otherwise) and $*$ denotes discrete convolution in the variable m. The function $g_e(x, t, s)$ represents the probability that the parent electron does not ionize within time t, and it is given as:

$$
g_e(x, t, s) = u\left(t - \frac{w-x}{v_e}\right) \int_w^\infty h_e(\xi; x, s)d\xi, \quad \text{(3)}
$$

where $u(x)$ is the unit step function. Similarly, if we start with a parent hole, we obtain another recursive equation

$$
\begin{aligned}
f_h(m, t; x, s) = \quad & g_h(x, t, s)\delta_{m-1} \\
& + \int_0^x [f_h(m, t - \tau_h; \xi, s + \tau_h) * f_h(m, t - \tau_h; \xi, s + \tau_h) \quad \text{(4)} \\
& * f_e(m, t - \tau_h; \xi, s + \tau_h)]h_h(\xi; x, s)d\xi,
\end{aligned}
$$

where $g_h(x, t, s)$ is the probability that the parent hole does not ionize at within time t, and it is given by

$$g_e(x,t,s) = u\left(t - \frac{w-x}{v_e}\right) \int_w^\infty h_e(\xi;x,s)d\xi \,. \text{ (5)}$$

The coupled pair of recursive equations in (2) and (4), which fully characterize the PDFs f_e and f_h, can be solved numerically to determine the joint PDF $f_{G_s,T_s}(m,t,s)$. However, the discrete convolution under the integrals can be simplified to multiplication using the z-transform properties. Let $F_e(z,t;x,s)$ and $F_h(z,t;x,s)$ be the z-transforms of $f_e(m,t;x,s)$ and $f_e(m,t;x,s)$ with respect to the variable m. More precisely, if we define

$$F_e(z,t;x,s) = \sum_{k=0}^\infty f_e(k,t;x,s)z^k$$
$$F_h(z,t;x,s) = \sum_{k=0}^\infty f_h(k,t;x,s)z^k \,, \qquad \text{(6a)(6b)}$$

for all complex $|z| \le 1$, then the discrete recursive equations defined in (2) and (4) can be simplified to

$$\begin{aligned} F_e(z,t;x,s) &= g_e(x,t,s)z + \int_x^w F_e^2(z,t-\tau_e;\xi,s+\tau_e) \\ &\quad \times F_h(z,t-\tau_e;\xi,s+\tau_e)h_e(\xi;x,s)d\xi, \\ F_h(z,t;x,s) &= g_h(x,t,s)z + \int_0^x F_h^2(z,t-\tau_h;\xi,s+\tau_h) \\ &\quad \times F_e(z,t-\tau_h;\xi,s+\tau_h)h_h(\xi;x,s)d\xi. \end{aligned} \qquad \text{(7)}$$

After solving the coupled recursive equations numerically over $z = e^{-j\omega}(-\pi < \omega \le \pi)$, $t \ge 0$, $x \in [0,w]$ and $s \in [0,Tb]$, while using the time shifting and scaling properties of the z-transform, we obtain the z-transform (with respect to variable m), F_{G_s,T_s}, of the joint distribution f_{G_s,T_s} of the random variables G_s and T_s. More precisely,

$$F_{G_s,T_s}(z,t;s) = \sqrt{z}F_h(\sqrt{z},t;w,s) \,. \text{ (8)}$$

The joint PDF can then be found by using the inversion formula [24], i.e., by evaluating the z-transform on the unit circle and find its Fourier series coefficients

$$f_{G_s,T_s}(m,t;s) = \frac{1}{2\pi} \int_{-\pi}^\pi F_{G_s,T_s}(e^{j\omega},t;s)e^{-j\omega n}d\omega \,. \text{ (9)}$$

SECTION III. Numerical Calculation of the Age-Dependent Joint PDF of the Gain and Buildup Time

Consider an InGaAs-InP APD with a multiplication layer of width $w = 200$ nm. The APD is dynamically biased with a sinusoidal reverse voltage of the form $V_B(t) = B + C\sin(2\pi f_b t + \psi)$, where f_b is the bit transmission rate, i.e., $f_b = 1/T_b$, and T_b is the optical pulse window. The probability density functions of the free path, $h_e(\xi;x,s)$ and $h_h(\xi;x,s)$, were calculated according to the dead-space multiplication theory (DSMT) as described in [21]. The calculation of the free path's probability density functions requires the knowledge of the ionization coefficients and ionization-threshold energies for the InP multiplication region, which can be extracted from [25]. Our main goal is to select the sinusoidal parameters for optimal receiver performance. As an example, the peak-to-peak and the DC parameters of the sinusoidal-biasing parameters were selected as $B = 13$V, $C = 6$V and $\psi = 0$. The sinusoidal-biasing period is equal to 5.5 transit times, which is equivalent to a data rate of $f_b = 60$Gb/s. The electron and hole saturation velocity are approximated as $v_e = v_h = 0.67 \times 10^7$cm/s.

We first solve numerically the coupled recursive equations (7) using a simple iterative method. Next, the joint PDF of the random gain and G_s and the random buildup time Tswere calculated from (9). Fig. 2 shows examples of the age-dependent joint PDF $f_{G_s,T_s}(m,t,s)$ calculated for different values of the age variable, $s = 0$, $s =$

$T_b/4$ and $s = 3T_b/4$. The hole transit time is simply $w/v_h = 3.0$ps. The correlation between the gain and the buildup time is clear from the joint PDF plots in agreement with the behavior of the static bias case [15]. The numerical calculations show that the arrival time of the incident photon to the multiplication region, s, plays a key role in the distribution function, a property that is heavily exploited in reducing the buildup time for optical receivers by adjusting the arrival time, s, of the incident photon relative to dynamic-bias cycle. For instance, by examining the shape of the PDF, the age-dependent joint PDF of an avalanche triggered by a photon arrived at the beginning of the pulse ($s = 0$), is expected to have a higher mean gain ($E[G_s]$) and longer mean buildup time ($E[T_s]$) compared to a photon arrived at a later time (e.g., $s = 3T_b/4$).
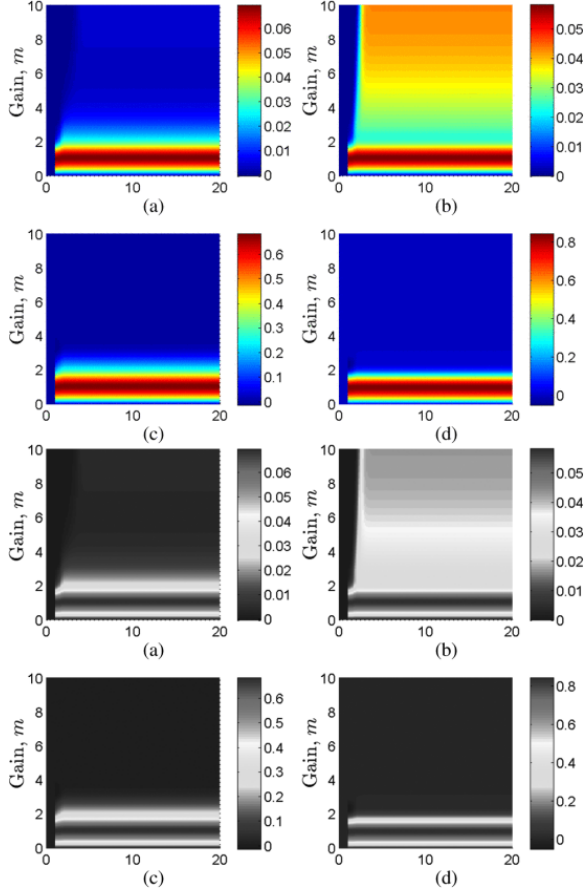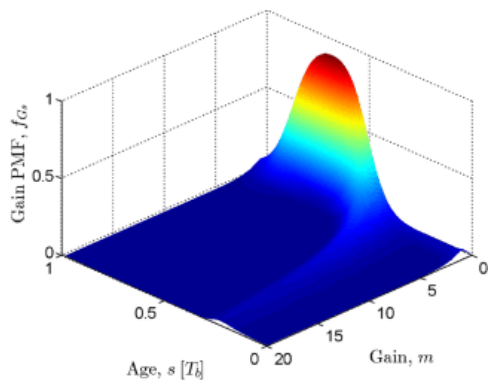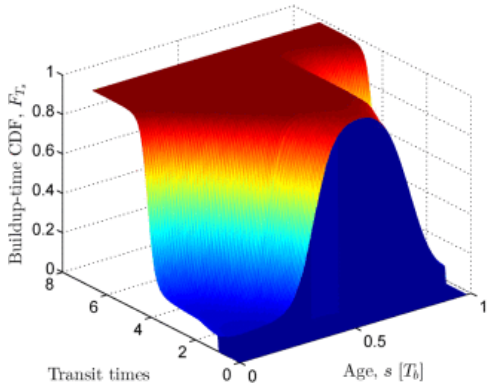

Fig. 2. Joint PDF fGs,Ts of the stochastic gain G_s and the stochastic buildup time T_s for an InP APD with a 200-nm multiplication layer. Fig. 2(a)–(d) correspond to different initiating parent hole of age $s = 0$, $s = 0.25T_b$, $s = 0.5T_b$ and $s = 0.75T_b$, respectively. The reverse dynamic voltage bias is of the form $V_b(t) = 13 + 6\sin(2\pi t/T_b)$, where T_b is the bit duration with $1/T_b \approx 60$Gb/s.
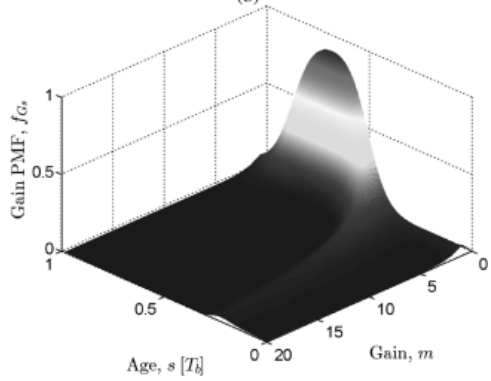
In order to better understand the effect of the incident photon's arrival age, s, the probability mass function (PMF) of the stochastic gain G_s can be found by taking the limit of the joint PDF as t approaches infinity, i.e., $f_{G_s}(m, s) = \lim_{t\to\infty} f_{G_s, T_s}(m, t, s)$. The result is shown in Fig. 3(a). Furthermore, the cumulative distribution function (CDF) of the stochastic buildup time T_s [Fig. 3(b)] as a function of the age, s can be found as follows: $F_{T_s}(t, s) = \sum_{m=1}^{\infty} f_{G_s, T_s}(m, t, s)$. Fig. 3(a) shows a high mean for the gain (accompanied by a larger spread) at the beginning of the period (at $s = 0$) and decreases to unity when s is around 70% of the bit period T_b. Moreover, the CDF of the buildup time shows a similar behavior in Fig. 3(b), where the expected buildup approaches a unit of transit time when the age, s is around $0.7T_b$. Recall that the minimum possible buildup time is the hole transit time w/v_h, i.e., $P\{T_s \leq 1\} = 0$. This feature is observed in Figs. 2 and 3(b).
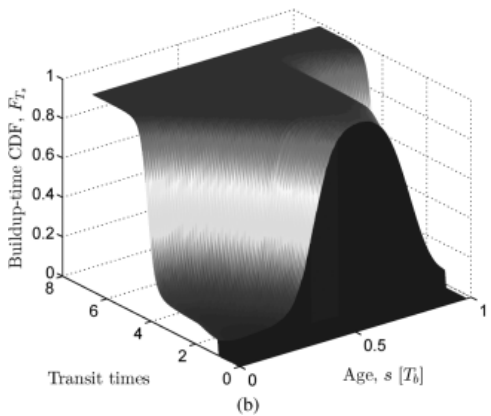
Fig. 3. Marginal distributions of the stochastic gain, G_s and the stochastic buildup time, T_s. (a) Marginal probability mass function (PMF) of the age-dependent stochastic gain, G_s, as a function of the initiating hole age, s (in bit duration window, T_b). (b) Marginal cumulative distribution function (CDF) of the age-dependent stochastic buildup time, T_s, as a function of the initiating hole age, s (in bit duration, T_b).
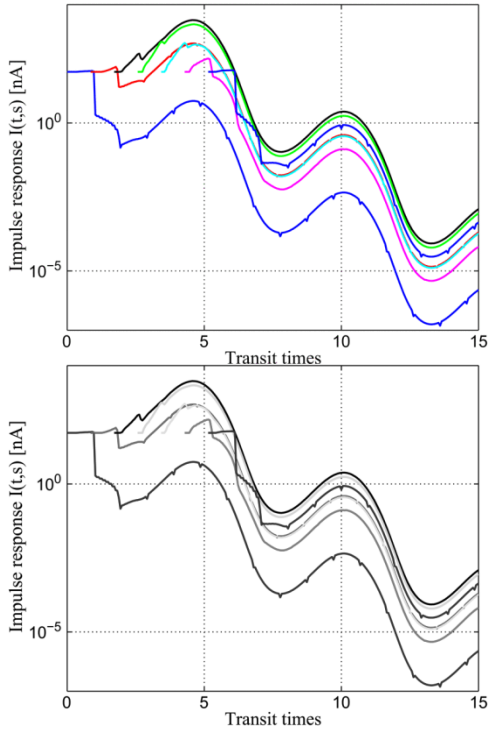
Fig. 4. Calculated age-dependent impulse response function under a sinusoidal dynamic bias for different ages (photon arrival time). The dynamic-biasing parameters used are: $B = 13$V, $C = 6$V, and $\psi = 0$.

For this example, the average gain calculated by Hayat and Ramirez [21] for this particular receiver is 28. The marginal density function of the gain (obtained by integrating the joint PDF over the buildup time) yields the mean of 26.7, which is in good agreement with the previous results found in [21].

We next use the joint PDF of G_s and T_s to calculate the statistical properties of the impulse-response function and investigate the effect of the dynamic reverse bias on ISI and receiver performance in high-speed digital receivers.

SECTION IV. Mean Impulse-Response Function

In this section, we introduce a novel model for the mean impulse-response function that facilitates the calculation of the receiver statistics once the age-dependent joint PDF of the gain and the buildup time has been determined. For the constant reverse bias, the mean impulse response, $i(t) = E[I(t)]$, and its second moment, $i_2(t) = E[I^2(t)]$, are known to decay exponentially at the same rate [26]. The calculation of the age-dependent impulse response function in the case of the dynamic bias is shown in Fig. 4 for different values of the age variable s. These curves were obtained by solving Eqs.(10a) and (10b) in [21] numerically using the method of iterations. Fig. 4 shows that the tail of the impulse response can be approximated by a decaying exponential function with a constant average rate, b. It is clear from the numerical calculations that the average decay rate, b, is independent of the carrier age, i.e., regardless of the arriving time of the photon with respect to the dynamic electric field the impulse response function decays at the same average rate. Moreover, the fluctuations in the tail can be ignored because we are interested in the asymptotic behavior of the impulse response, where the average decay rate exponent dominates the bounded sinusoidal fluctuations, i.e., $e^{-bt+\delta\sin(\omega_b t)} \approx e^{-bt}$ when t is large. With this in mind, we approximate the mean and the second moment of the impulse response as follows:

$$i(t,s) \approx a_s e^{-b(t-s)} u(t-s) \text{ (10a)}$$

and

$$i_2(t,s) \approx c_s e^{-b(t-s)} u(t-s), \text{ (10b)}$$

where a_s and c_s are age-dependent coefficients to be determined and b represents the average decaying rate of the impulse response tail. To see the effect of the dynamic biasing scheme on the ISI, we calculated the mean pulse-response function by integrating the age-dependent impulse responses over the age variable s in the interval $[0, T_b]$. Fig. 5 shows the calculated mean pulse response of a 200 nm multiplication region InP-based APD, when it is illuminated by a rectangular non-return-to-zero (NRZ) pulse. For simplicity, in this example we assume a uniformly distributed random stream of photons. Two cases are considered: sinusoidal dynamic bias and a constant reverse bias. In this example the width of the optical pulse is 16.5 ps (consistent with 60-Gb/s NRZ bit stream). The reduction in the tail of the pulse response in the dynamic-bias case is clearly evident compared with that for the constant-bias case.The total mean gain generated by the pulse under dynamic-biasing is 27 and its bandwidth is 80 GHz, giving rise to an average GBP (i.e., the GBP averaged over the age variable s in the interval $[0, T_b]$) of 2,161 GHz, which is compared to 437 GHz in the constant-bias case as pointed out in [21]. This shows that a dynamically biased APD can increase the pulse-response gain-bandwidth product of an APD by a factor of 5.
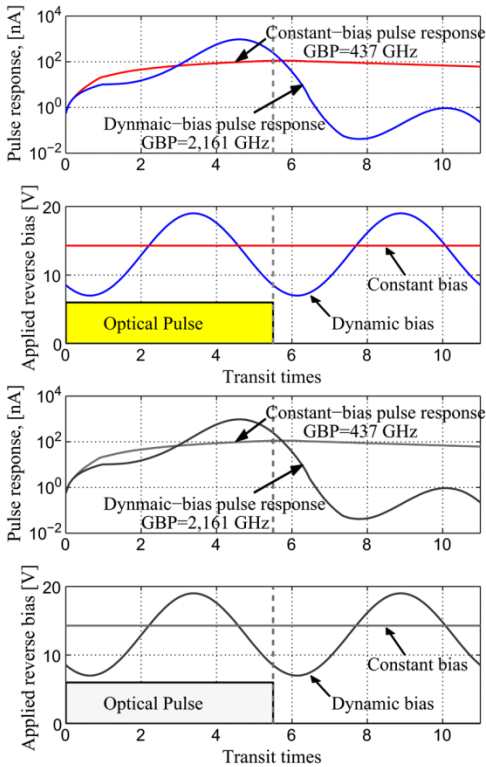
Fig. 5. Calculated time response to an 16.5-ps rectangular optical pulse of dynamically biased APD, with a sinusoidal-dynamic bias function as shown, and a conventional InP APD. A five-fold enhancement in the GBP is predicted.

By overlaying sweeps of different segments of a long data stream, an eye diagram can be simulated. We consider $2^{13} - 1$ NRZ bits with a pulse width of 25 ps as in a 40-Gb/s NRZ bit stream. Fig. 6 shows the simulated eye diagram of the 200 nm multiplication region APD, once with the sinusoidal dynamic-field (upper plot) and once with the static reverse bias (lower plot). We observe that in the presence of channel noise, the eye opening of the sinusoidal-bias case is wide open compared to that for the static-bias case. This shows that dynamically biased APD can increase the receiver performance substantially compared to the same APD operated under the

conventional static biasing scheme. Note that, the shape of the eye diagram for dynamic-bias case is different from that of the conventional OOK NRZ. This result is expected since dynamic biasing provides strong avalanche current in the early phase of the optical-pulse window followed by a much weaker impact ionization that terminates the avalanche current with high probability before the start of next bit. This can also be realized in the logarithmic plot of the pulse response depicted in 5.
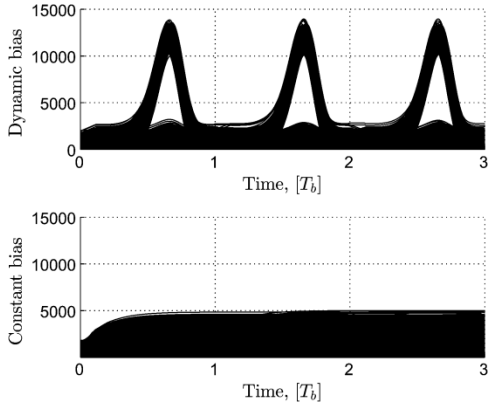

Fig. 6. Receiver eye diagram of a 200 nm InP dynamically biased APD (upper plot) compared to the traditional constant-biasing APD (lower plot) for an OOK communication system operating at 40 Gb/s.

Our next step is to explore the physical meaning of the age-dependent coefficients, a_s and c_s and the decay rate b introduced in (10) . Following [15], we approximate the stochastic impulse-response, $I(t,s)$ by a specified shape function that is parameterized by the age-dependent random gain G_s and the age-dependent random buildup time T_s. An example of such a function is the rectangular random-duration (RD) with random height qG_s/T_s and random duration T_s, where q is the electronic charge. Note that the area under this function is qG_s. The randomness in the impulse-response functions area represents the gain uncertainty and the randomness in its duration represents the uncertainty in the buildup time. This parametric approach for representing the stochastic impulse-response function significantly simplifies the complexity of the impulse-response function while maintaining the key features that govern the random gain, the excess-noise and speed properties of the APD. (Non-rectangular shape functions have also been considered [15].) Therefore,

$$\int_s^\infty i(t,s)dt \approx \int_s^\infty a_s e^{-b(t-s)} = \frac{a_s}{b} \text{ and}$$

$$\mathrm{E}\left[\int_s^\infty I_p(t,s)\mathrm{d}t\right] \tag{11)(12}$$

$$\approx \mathrm{E}\left[\int_s^\infty q\frac{G_s}{T_s}(u(t-s)-u(t-s-T_s))\mathrm{d}t\right] = q\mathrm{E}[G_s],$$

and by equating the above two equations, we conclude that $a_s = qb\mathrm{E}[G_s]$. Unlike the static-bias case, the statistics of the buildup time and gain of an APD operating under dynamic reverse bias will vary cyclically with time with a period equal to the dynamic field period; therefore, a_s is periodic in s with a period equal to bit duration and to the dynamic reverse voltage period T_b. Similarly, the parameter c_s of the second moment, $i_2(t,s)$, can be found as follows:

$$\int_s^\infty i_2(t,s)dt \approx \int_s^\infty c_s e^{-b(t-s)} = \frac{c_s}{b} \text{ and}$$

$$\mathsf{E}\left[\int_s^\infty I_p^2(t,s)\mathrm{d}t\right] \tag{13)(14}$$

$$\approx \mathsf{E}[\int_s^\infty q^2 \frac{G_s^2}{T_s^2}(u(t-s)-u(t-s-T_s))\mathrm{d}t] = q^2\mathsf{E}\left[\frac{G_s^2}{T_s}\right].$$

As a result, $c_s = q^2 b\mathsf{E}[G_s^2/T_s]$.

We now proceed to characterize the decay rate, b. By comparing the exact expression(30) and its simplification (31) for the photocurrent variance, as derived in theAppendix, we can relate the decay rate to the statistics of the impulse response G_s and T_s as follows:

$$b = \frac{2\int_0^{T_b} \mathsf{E}[G_s^2/T_s]ds}{\int_0^{T_b} \mathsf{E}[G_s^2]ds} . \tag{15}$$

We note that for a static-bias case, the dependence on the age variable s will be absent in G_s and T_s, and the parameters a_s, c_s, and b of the approximated impulse response statistics collapse to their static-field counterparts reported in [15] [Eqs. (11), (26) and(29)]. In the next section, we use the impulse-response-function approximations described above to determine the receiver performance of an APD operating with a dynamically reversed bias. We particularly investigate the effect of the different bias settings (DC level, peak-to-peak value and phase) on the receiver BER.

SECTION V. Receiver Performance Analysis Under Dynamic Reverse Biasing

In this section, we develop expressions for the statistics of the output of an APD-based integrate-and-dump receiver operating under dynamic biasing. We will consider an arbitrary past bit-pattern of length L bits and calculate the mean and the variance of the photocurrent and the receiver output conditional on the value of the current bit while taking into account the ISI contributions from past bits. This is done by adding up the contributions from the past bits in the pattern to the present bit. Next, by averaging over all possible past bit-patterns, we determine the average BER. The analysis developed here offers closed-form expressions for the mean and variance of a dynamically biased APD receiver's output, with well-defined parameters that capture ISI, Johnson noise and the APD's speed.

A. Output of the Integrate-and-Dump Receiver

Consider a modulated optical photon stream with a bit duration T_b. The photocurrent generated by the dynamically biased APD is fed into a bit integrator that is synchronized with the optical stream. Let Γ_n be the integrate-and-dump receiver output when the nth past bit is "1" and all other past bits are "0" (including the present bit). The mean of the receiver output can be expressed as

$$\langle \Gamma_n \rangle = \phi \int_0^{T_b} \int_{-nT_b}^{-(n-1)T_b} i(t,s)dsdt, \tag{16}$$

where ϕ is the average photon absorption rate by the detector. Note that, the average photon absorption rate can be defined as $\phi = \eta\Phi$, where η is the quantum efficiency of the APD defined as the probability that a single photon incident generates an impulse response and Φ is the photon flux incident on the photodetector. Using the parametric model of the mean impulse response described in Section IV, the mean of the nth bit photocurrent output can be shown to be

$$\mu_n = \langle \Gamma_n \rangle = \frac{\phi e^{-nbT_b}}{b}(e^{bT_b} + e^{-bT_b} - 2)\sum_{k=-\infty}^{\infty}\frac{A_k}{j2\pi k f_b + b},$$

where the A_k's are the Fourier series coefficients of the periodic function a_s with $A_k = T_b^{-1}\int_0^{T_b} a_s e^{-j2\pi ks/T_b}ds$. To calculate the variance of Γ_n, we undertake a cyclostationary stochastic analysis shown in the Appendix. This results in

$$\sigma_{\Gamma_n}^2 = \frac{2\phi}{b^2}e^{-nbT_b}(e^{bT_b} - 1)(1 - e^{-bT_b} - bT_b e^{-bT_b})$$
$$\times \sum_{k=-\infty}^{\infty}\frac{C_k}{b + j2\pi k f_b}, \quad (17)$$

where C_k's represent the Fourier series coefficients of the periodic function c_s with $C_k = T_b^{-1}\int_0^{T_b} c_s e^{-j2\pi k f_b s}ds$. Now consider an arbitrary past bit pattern, I_j, of length L representing the transmitted information. The bit-length parameter, L, can be chosen to be sufficiently large to capture all the previous bits that has significant impacts on the current output; an appropriate value of L can be determined in practice by trial and error. To calculate the mean of the receiver output for the bit pattern I_j when the present bit is zero, we add up the contributions from each non-zero past bits in the pattern, which yields the expression

$$\mu_{\Gamma|0}(I_j) = \sum_{n=1}^{2^L}u_n(I_j)\mu_n, \quad (18)$$

where $u_n(I_j)$ is 1 when the nth bit in the pattern I_j is a "1" bit and I_j is 0 otherwise.

Similarly, one can calculate the variance of the receiver output associated with the pattern I_j while conditioning on the first bit being 0 bit by adding up the contributions from the non-zero past bits as well as contribution from Johnson noise and obtain

$$\sigma_{\Gamma|0}^2(I_j) = \sum_{n=1}^{2^L}u_n(I_j)\sigma_{\Gamma_n}^2 + \sigma_J^2. \quad (19)$$

Next, the mean and variance of the receiver output when the present bit is 1 are found by adding the contributions from the photons in the present bit to $\mu_{\Gamma|0}$ and $\sigma_{\Gamma|0}^2$, respectively. The contribution to the mean of the receiver output from the photons available in the present bit (for $n = 0$) is

$$\mu_0 = \phi\int_0^{T_b}\int_0^t i(t,s)dsdt = \phi\frac{A_0}{b^2}(bT_b - 1 + e^{-bT_b})$$
$$+ \phi\sum_{\substack{k=-\infty\\k\neq 0}}^{\infty}\frac{A_k}{b(j2\pi k f_b + b)}(e^{bT_b} - 1). \quad (20)$$

The contribution to the variance of the receiver output from the photons available in the present bit is

$$\sigma_0^2 = \phi \int_0^{T_b} \int_0^{T_b} \int_0^{t_1 \wedge t_2} R_I(t_1, t_2, s) ds dt_1 dt_2$$

$$= \phi \frac{2C_0}{b^3}[bT_b + bT_b e^{-bT_b} + 2e^{-bT_b} - 2] + \sum_{\substack{k=-\infty \\ k \neq 0}}^{\infty} \frac{2\phi C_k}{b + j2\pi f_b k}$$

$$\times [\frac{e^{-bT_b} - 1}{b(b + j2\pi f_b k)} + \frac{bT_b e^{-bT_b} + e^{-bT_b} - 1}{b^2}].$$

Finally, when we combine μ_0 and σ_0^2 with the contribution from the previous bits (μ_n and σ_n^2 for $n = 1, 2, \cdots$), we obtain the mean and the variance of the receiver output associated with the pattern I_j conditioning on the present bit being 1. More precisely,

$$\mu_{\Gamma|1}(I_j) = \mu_{\Gamma|0}(I_j) + \mu_0, \text{ (21)}$$

and

$$\sigma_{\Gamma|1}^2(I_j) = \sigma_{\Gamma|0}^2(I_j) + \sigma_0^2. \text{ (22)}$$

A common approximation for the receiver output is the Gaussian distribution [27]. By conditioning on the transmitted bit, the conditional distribution of the receiver output for a specific pattern I_j, is assumed to be Gaussian with mean $\mu_{\Gamma|i}(I_j)$ and variance $\sigma_{\Gamma|i}^2(I_j)$ for $i \in \{0,1\}$. Therefore, for every pattern, I_j, the pattern-specific BER is

$$\text{BER}(I_j) = \frac{1}{4}[\text{erfc}(\frac{\theta - \mu_{\Gamma|0}(I_j)}{\sigma_{\Gamma|0}\sqrt{2}}) + \text{erfc}(\frac{\mu_{\Gamma|1}(I_j) - \theta}{\sigma_{\Gamma|1}\sqrt{2}})],$$

where θ is the decision threshold. In practice, θ is optimized to minimize the overall BER. In the next section, we show an efficient method to determine θ. By assuming an equiprobable distribution on the past bits, the overall BER is calculated by averaging over all possible bit patterns. More precisely,

$$\text{BER} = \frac{1}{2^L}\sum_{j=1}^{2^L} \text{BER}(I_j). \text{ (23)}$$

B. The Decision Threshold, $\boldsymbol{\theta}$

The derivation of the BER expressions involves the computation of the decision threshold, θ, i.e., the optimized threshold that minimizes the overall BER. The optimal decision threshold can be characterized analytically by setting the derivative of the BER with respect to the decision threshold to zero. As a result, we obtain

$$\sum_{j=1}^{2^L} e^{-\frac{(\mu_{\Gamma|1}(I_j) - \theta)^2}{2\sigma_{\Gamma|1}^2(I_j)}} / \sigma_{\Gamma|1}(I_j) = \sum_{j=1}^{2^L} e^{-\frac{(\theta - \mu_{\Gamma|0}(I_j))^2}{2\sigma_{\Gamma|0}^2(I_j)}} / \sigma_{\Gamma|0}(I_j). \text{ (24)}$$

Unfortunately, the obtained result cannot be solved analytically; however, the optimal decision threshold can be determined numerically by means of an exhaustive search. Here we report a convenient analytical approximation to the optimal threshold. Let $\bar{I} = \arg \max_{I_j} \mu_{\Gamma|0}(I_j)$ and $\underline{I} = \arg \min_{I_j} \mu_{\Gamma|1}(I_j)$. It is clear that the

left hand side of [(24)](#) is dominated by the exponent $(\mu_{\Gamma|1}(\underline{I}) - \theta)^2/2\sigma_{\Gamma|1}^2(\underline{I})$ and the right hand side is

dominated by $(\theta - \mu_{\Gamma|0}(\overline{I}))^2/2\sigma_{\Gamma|0}^2(\overline{I})$. Thus, by equating the dominant terms, the decision threshold $\hat{\theta}$ can be approximated by

$$\hat{\theta} = \frac{\sigma_{\Gamma|0}(\overline{I})\mu_{\Gamma|1}(\underline{I}) + \sigma_{\Gamma|1}(\underline{I})\mu_{\Gamma|0}(\overline{I})}{\sigma_{\Gamma|0}(\overline{I}) + \sigma_{\Gamma|1}(\underline{I})} . \quad (25)$$

Note that $\overline{I}$ and $\underline{I}$ represent the worst two-bit-pattern scenarios on the BER when the present bit is "0" and "1,"

respectively. The analytical decision threshold approximation, $\hat{\theta}$, is the intersection of the conditional probability density functions for these two worst bit-pattern scenarios.

SECTION VI. BER and Receiver-Sensitivity Results Under Dynamic Biasing

As before, we consider an InP-based APD with 200 nm multiplication layer. The transmission rate is 60 Gb/s. From the statistical analysis of the gain and buildup time derived in Section II, we calculate all the parameters of the model, which are summarized in Table I. Note that the statistics of the stochastic gain, G_s, and buildup time, T_s, are averaged over all possible arrival ages of the incident photon, s.

TABLE I Avalanche Process Statistics of an InP APD

$E[G_s]$	27.46	$E[\ ]$	3.689×10^3
$E\left[\dfrac{G_s^2}{T_s}\right]$	2.915×10^{14}	b	1.580×10^{11}
A_0	4.402×10^{-18}	C_0	7.482×10^{-24}

$E[G_s]$	27.46	$E[G_s^2]$	3.689×10^3
$E\left[\dfrac{G_s^2}{T_s}\right]$	2.915×10^{14}	b	1.580×10^{11}
A_0	4.402×10^{-18}	C_0	7.482×10^{-24}

In order to obtain the Johnson-noise level, we obtained the input noise current density, i_n, and bandwidth, B_{TIA} of the transimpedance amplifiers (TIAs) reported in [16]. The average of i_n for each transmission speed was fitted linearly to obtain the average, i_n as a function of transmission speed. The fit yielded the equation $i_n = 4.81 \times 10^{-10} R_b + 5.87 pA/\sqrt{Hz}$. Similarly, by fitting the average of B_{TIA} against transmission speed, we obtained the average B_{TIA} as a function of transmission speed, given by $B_{\text{TIA}} = 0.91 R_b$ GHz. Using these averaged i_n and B_{TIA} values, we were able to obtain the average Johnson-noise levels, σ_j, as a function of transmission speed using the formula $\sigma_j = (\sqrt{B_{\text{TIA}} i_n^2}/q)(1/R_b)$.

As for the benefits of dynamic biasing on the BER, our numerical calculations predict an improvement by a factor of 10^6. For example, as shown in Fig. 7, assuming an average of 600 photons per pulse, our calculations show that the BER is 0.2 when using the traditional static biasing scheme at a transmission speed 60 Gb/s, which is way beyond the speed of this APD. On the other hand, if we use a dynamic biasing (DC level = 13V, 12 V peak-to-peak AC component with the sinusoids lagging the bit by 0.73 bit period), then the BER associated with the same APD operated at 60 Gb/s can be reduced astonishingly to 10^{-6}. These parameters were chosen, in part, so that the static and dynamic biasing schemes are equivalent from the average multiplication gain perspective. The average gain in our example is approximately 26 for all the peak-to-peak reverse bias voltages in Fig. 7. With that said, it is important to note that the benefit of sinusoidal basing is dependent upon the time offset between the optical pulse and the dynamic bias, as Fig. 7 shows. Fortunately, the optimal performance appears to be

robust with respect to errors in the offset if such errors occur in the implementation stage of the dynamic biasing. For example, an error of ±13% from the optimal phase lagging (between 0.6 and 0.86 bit period) guarantees a BER less than 10^{-5} for the receiver operating under dynamic bias with a 12 V peak-to-peak bias swing.
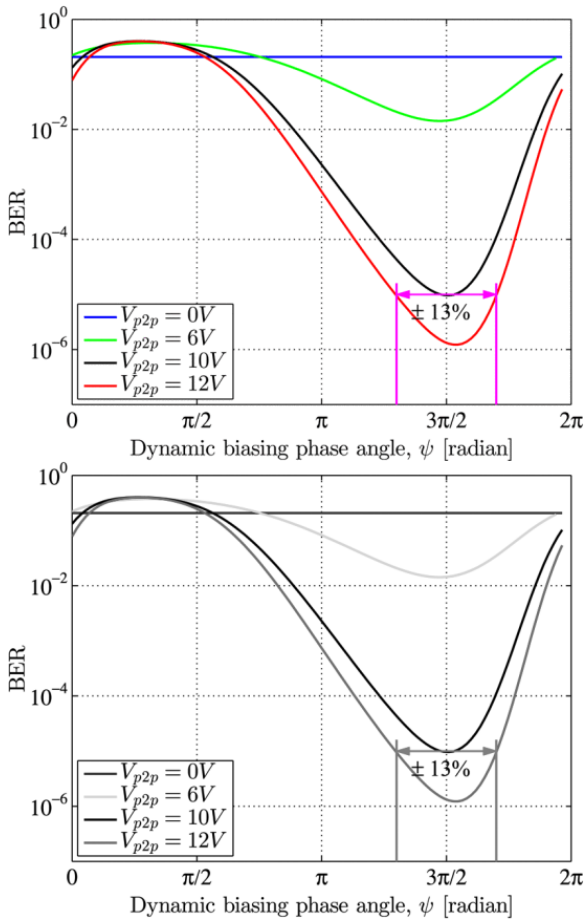

Fig. 7. Dependence of the BER of an InP-based APD with 200 nm multiplication width on the time delay between the optical piulse and the sinusoidal bias. Different peak-to-peak swings are shown. The average gain in all cases is approximately 26.

The BER calculated in Fig. 7 uses the approximated threshold $\hat{\theta}$ described earlier. However, the optimal BER can be found numerically using the conditional probability density functions of the receiver output. We compared the approximated decision threshold $\hat{\theta}$ with the numerical optimized BER. The results show that the BER found using the approximated decision threshold, $\hat{\theta}$, has almost the same performance as the optimized BER in the region of interest (when the phase is optimized). It turns out that the approximated threshold, $\hat{\theta}$, overestimates the BER by an error less than 1% when operating within ±13% from the optimal phase lagging as compared to the numerical threshold, θ.

We also examined the receiver sensitivity, defined as the minimum optical power (or average number of photons per bit) needed to achieve a BER of 10^{-12}. Sensitivity-versus-gain curves were calculated for different peak-to-peak bias swings. The results are shown in Fig. 8 for a transmission speed of 60 Gb/s. The key observation is that by increasing the peak-to-peak voltage, the optimum sensitivity is reduced dramatically. Indeed, our calculations predict a reverse dynamic biasing can improve the receiver sensitivity −20 dBm at an

optimal gain of approximately 47 for a 60 Gb/s system when the peak-to-peak voltage is 12 V. Note that, as the peak-to-peak voltage increases, the optimal gain increases while providing a lower sensitivity due to the reduced avalanched buildup time caused by the dynamic nature of the reverse bias. In addition, we observe that by increasing the peak-to-peak voltage, the sensitivity to the optimal-gain values decreases. For instance, at 6 V peak-to-peak, the optimal gain region is around 12. However, as we increase the peak-to-peak voltage to 12, the receiver sensitivity becomes resilient to the optimal gain. For example, the receiver sensitivity is less than −20 dBm when the average gain is between 30 and 70. This too is a benefit of the dynamic-biasing scheme, which offers substantial increase in the avalanche gain while maintaining a short avalanche buildup time. It is worth to mention that this device cannot operate with the conventional (static) reverse bias with such transmission speeds. The calculated BER for the static reverse bias at 60 Gb/s was in the range of 10^{-1} even for large input power (sensitivity > 0 dBm). The analysis in this paper ignores the tunneling current caused by the high electric field in the multiplication region. However, generalizing the receiver output statistics to include the tunneling effects can be carried out in a straightforward fashion using the techniques reported in [16]. Of course, in practice, the benefits of the dynamic biased will be reduced when the tunneling current becomes dominant.
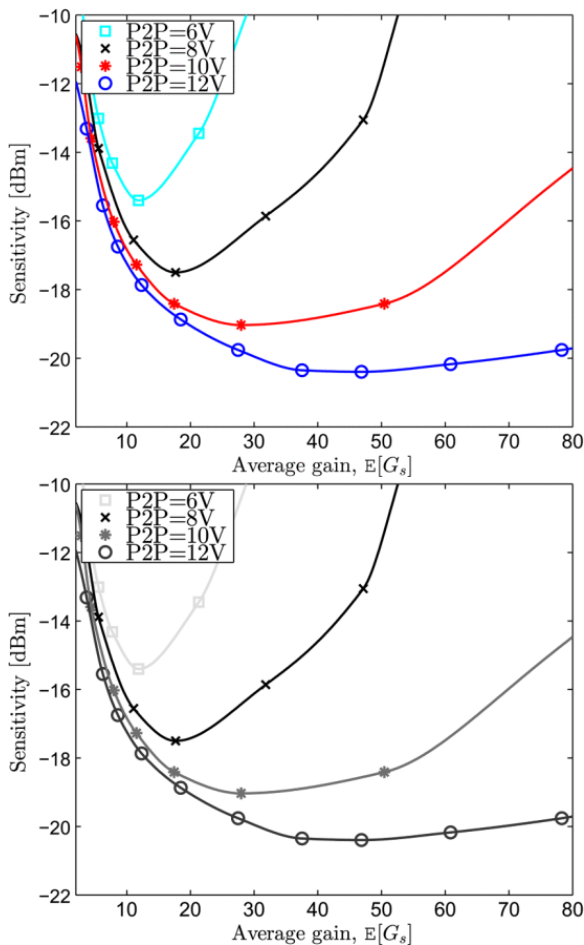

Fig. 8. Receiver sensitivity versus gain for the dynamically biased 200-nm InP APDs investigated for a 60 Gb/s transmission system and for different peak-to-peak voltage swings in the dynamic bias.

SECTION VII. Conclusion

We have developed a method to predict the performance of APD-based receivers operating under dynamic biasing that is synchronized with the incoming bit stream. To do so, the statistical correlation between the stochastic gain the stochastic avalanche buildup time in dynamically biased APDs was determined. We incorporated these results with modified point-process analysis that accommodated the dynamic nature of the

APD's bias to derive compact expressions for the output of an integrate-and-dump receiver in an OOK direct-detection system. The results drawn here include the effects of ISI and the dead space. The closed-form expressions for APD receiver output operating under dynamic reverse biased can be used to properly select the DC level, peak-to-peak value and phase of a dynamic reverse bias to yield the optimal receiver sensitivity. The calculations had shown that dynamic biasing operating at the optimal settings improves the receiver performance beyond its traditional limits inherited from the notoriously long buildup times of InP APD under conventional static biasing. Indeed, our calculations predicted a reverse dynamic biasing can improve the receiver sensitivity for InP APDs with 200 nm multiplication region from 0 dBm to −20 dBm at an optimal gain of approximately 47 for a 60 Gb/s system when the peak-to-peak voltage is set to 12 V compared to the conventional static reverse bias.

ACKNOWLEDGMENT

Appendix Photocurrent Generated by Dynamically Biased APD

The approach for determining the statistical properties of the photocurrent is based on the mathematical theory for filtered point processes [5], [28]. Specially, for the underlying point process, which represents the photon stream, we will consider a doubly stochastic Poisson point process, where the stochastic intensity is proportional to the instantaneous optical power of the received light at the receiver.

We examine the statistics of the photocurrent, $C(t)$, produced by a bit-synchronized dynamically biased APD generated by a random photoelectron flux with mean ϕ. Every photon absorbed that enters the multiplication region generates an age-dependent impulse response of electric current of charge qGs and time duration T_s. Therefore, a photon stream incident on an APD results in a stream of electrical impulse-response functions that add up together to generate an electric current $C(t)$. Assume that a photo-event (absorption of a photon and the creation of an electron-hole pair) generated at time s produces a random impulse response, $I(t, s)$. If the time axis is divided into incremental time intervals Δt, the number of photo-events in one time-interval follows a Poisson distribution with a mean $\phi \Delta t$. Thus, for a sufficiently small Δt, the Poisson distribution can be approximated by a Binomial distribution, where the probability p that a photo-event occurs within an interval is $p = \phi \Delta t$. The electric current is written as $C(t) = \lim_{\Delta t \to 0} \sum_s X_s I(t, s\Delta t)$, where X_s has a value 1 with probability p and it is 0 otherwise. This sequence represents the existence of a photocurrent at the instant $s\Delta t$. The random variables, X_s, are independent with a mean value $\langle X_s \rangle = p$. The mean of the product $X_s X_k$ is p for $s = k$ and p^2 otherwise. The first and second moments of p^2 become

$$
\begin{aligned}
\mathsf{E}[C(t)] \quad &= \lim_{\Delta t \to 0} \sum_s p\, i(t, s\Delta t), \\
\mathsf{E}[C^2(t)] \quad &= \lim_{\Delta t \to 0} \sum \sum_{s \neq k} p^2 \mathsf{E}[I(t, s\Delta t)]\mathsf{E}[I(t, k\Delta t)] \quad \text{(26)(27)} \\
&\quad + \lim_{\Delta t \to 0} \sum_s p\, \mathsf{E}[I^2(t, s\Delta t)].
\end{aligned}
$$

By substituting $p = \phi \Delta t$ and taking the limit $\Delta t \to 0$, the first and second moment of the photocurrent become

$$
\begin{aligned}
\mathsf{E}[C(t)] \quad &= \phi \int_{-\infty}^{\infty} i(t, s)\,ds = \phi \int_{-\infty}^{t} i(t, s)\,ds, \\
\mathsf{E}[C^2(t)] \quad &= \left(\phi \int_{-\infty}^{t} i_p(t, s)\,ds\right)^2 + \phi \int_{-\infty}^{t} i_2(t, s)\,ds, \quad \text{(28)(29)}
\end{aligned}
$$

where $i(t, s) = E[I(t, s)]$ and $i_2(t, s) = \mathsf{E}[I^2(t, s)]$. As a result the variance of $C(t)$ can be found as follows:

$$\sigma_{\hat{c}}^2(t) = \mathsf{E}[\mathcal{C}^2(t)] - \mathsf{E}[\mathcal{C}^2(t)]^2 = \phi \int_{-\infty}^{t} i_2(t,s)ds. \text{ (30)}$$

The calculation of the variance of the photocurrent generated by an APD requires knowledge of the second moment of the APD's impulse response, $i_2(t,s)$. However, calculation of the second-order statistics of $I(t,s)$ are generally computationally intensive. To overcome this complexity, one approach is to ignore the randomness in the shape of the impulse response function. For example, the variance of the photocurrent was found in [5] by assuming a deterministic shape proportional for the mean impulse response function.

Let $\hat{I}(t,s)$ be the simplified impulse response with a deterministic shape such as $\hat{I}(t,s) = G_s h(t-s)$, where G_s is the random gain generated by a photoevent at time s and $h(t)$ is the normalized (with an area q) function that represents the deterministic shape of the impulse response. Note that the deterministic shape $\hat{I}(t,s)$ is similar to the mean impulse response function approximation found in Section IV.

Substituting $\hat{I}(t,s)$ in (26) and (27), the first and second moment of the photocurrent become

$$\mathsf{E}[\mathcal{C}(t)] = \lim_{\Delta t \to 0} \sum_{s} p\mathsf{E}[G_s]h(t-s\Delta t),$$

$$\mathsf{E}[\mathcal{C}^2(t)] = \lim_{\Delta t \to 0} \Sigma \sum_{s \neq k} p^2 \mathsf{E}[G_s]\mathsf{E}[G_k]h(t-s\Delta t)h(t-k\Delta t)$$
$$+ \lim_{\Delta t \to 0} \sum_{s} p\mathsf{E}[G_s^2]h^2(t-s\Delta t).$$

As before by taking the limit $\Delta t \to 0$, the simplified variance of the photocurrent becomes

$$\hat{\sigma}^2(t) = \phi\mathsf{E}[G^2(t)] * h^2(t), \text{ (31)}$$

where * represents convolution.

References

1. C. H. Tan, J. S. Ng, S. Xie, J. P. R. David, "Potential materials for avalanche photodiodes operating above 10 Gb/s", *Proc. 4th Int. Conf. CODEC*, pp. 1-6, 2009.

2. A. Momtaz et al., "A fully integrated sonet OC-48 transceiver in standard CMOS", *IEEE J. Solid-State Circuits*, vol. 36, no. 12, pp. 1964-1973, Dec. 2001.

3. J. Cao et al., " OC-192 transmitter and receiver in standard 0.18- \$\mutextrm{m}\$ CMOS ", *IEEE J. Solid-State Circuits*, vol. 37, no. 12, pp. 1768-1780, Dec. 2002.

4. T. Torikai, T. Nakata, T. Kato, K. Makita, "40-Gbps waveguide APD", *Optical Fiber Communication Conf. Exposition/Nat. Fiber Optic Engineers Conf.*, Mar. 2005.

5. B. E. A. Saleh, M. C. Teich, Fundamentals of Photonics, New York, NY, USA:Wiley, pp. 644-695, 1991.

6. Y. S. Wang et al., "10-Gb/s planar InGaAs P-I-N photodetectors", *IEEE Sensors J.*, vol. 10, no. 10, pp. 1559-1563, Oct. 2010.

7. G. Wang et al., "Highly reliable high performance waveguide-integrated inp/ingaas pin photodiodes for 40 Gbit/s fibre-optical communication application", *Electron. Lett.*, vol. 39, no. 15, pp. 1147-1149, Jul. 2003.

8. G. P. Agrawal, Fiber-Optic Communication Systems, New York, NY, USA:Wiley-Interscience, 2002.

9. R. G. Smith, S. D. Personick, "Receiver design for optical fiber communications systems" in Semiconductor Devices for Optical Communication, New York, NY, USA:Springer-Verlag, 1980.

10. S. R. Forrest, "Sensitivity of avalanche photodector receivers for high-bit-rate long-wavelength optical communication systems" in Semiconductor and Semimetals, Orlando, FL, USA:Academic, vol. 22, 1985.

11. S. D. Personick, "Receiver design for digital fiber-optic communication systems I", *Bell Syst. Tech. J.*, vol. 52, no. 6, pp. 843-874, Jul./Aug. 1973.

12. S. D. Personick, "Receiver design for digital fiber-optic communication systems II", *Bell Syst. Tech. J.*, vol. 52, no. 6, pp. 875-886, Jul./Aug. 1973.

13. T. Nakata, T. Takeuchi, I. Watanabe, K. Makita, T. Torikai, "10 Gbit/s high sensitivity low-voltage-operation avalanche photodiodes with thin InAlAs multiplication layer and waveguide structure", *Electron. Lett.*, vol. 36, no. 24, pp. 2033-2034, Nov. 2000.

14. S. Hwang et al., "Design and fabrication of a 10 Gb/s InGaAs/InP Avalanche Photodiode (APD) based on the non-local model", *Proc. Int. Conf. IPRM*, pp. 215-218, May 2004.

15. P. Sun, M. Hayat, B. E. A. Saleh, M. Teich, "Statistical correlation of gain and buildup time in APDs and its effects on receiver performance", *J. Lightw. Technol.*, vol. 24, no. 2, pp. 755-768, Feb. 2006.

16. D. S. G. Ong, J. S. Ng, M. M. Hayat, P. Sun, J. P. R. David, "Optimization of InP APDs for high-speed lightwave systems", *J. Lightw. Technol.*, vol. 27, no. 15, pp. 3294-3302, Aug. 2009.

17. P. Sun, M. Hayat, A. Das, "Bit error rates for ultrafast apd based optical receivers: Exact and large deviation based asymptotic approaches", *IEEE Trans. Commun.*, vol. 57, no. 9, pp. 2763-2770, Sep. 2009.

18. M. M. Hayat et al., "Gain-bandwidth characteristics of thin avalanche photodiodes", *IEEE Trans. Electron Devices*, vol. 49, no. 5, pp. 770-781, May 2002.

19. C. Lenox et al., "Thin multiplication region inalas homojunction avalanche photodiodes", *Appl. Phys. Lett.*, vol. 73, no. 6, pp. 783-784, Aug. 1998.

20. S. Wang et al., "Low-noise avalanche photodiodes with graded impact-ionization-engineered multiplication region", *IEEE Photon. Technol. Lett.*, vol. 13, no. 12, pp. 1346-1348, Dec. 2001.

21. M. M. Hayat, D. A. Ramirez, "Multiplication theory for dynamically biased avalanche photodiodes: New limits for gain bandwidth", *Opt. Exp.*, vol. 20, no. 7, pp. 8024-8040, Mar. 2012.

22. M. M. Hayat et al., *Impact ionization devices under dynamic electric fields* , Nov. 2011.

23. G. El-Howayek, M. M. Hayat, "Method for performance analysis and optimization of APD optical receivers operating under dynamic reverse bias", *Proc. IEEE Photon. Conf.*, pp. 362-363, Sep. 2013.

24. R. M. Gray, J. W. Goodman, Fourier Transforms: An Introduction for Engineers, New York, NY, USA:Academic, 1995.

25. L. J. J. Tan, J. S. Ng, C. H. Tan, J. P. R. David, "Avalanche noise characteristics in submicron InP diodes", *IEEE J. Quantum Electron.*, vol. 44, no. 4, pp. 378-382, Apr. 2008.

26. M. M. Hayat, B. E. A. Saleh, "Statistical properties of the impulse response function of double-carrier multiplication avalanche photodiodes including the effect of dead space", *J. Lightw. Technol.*, vol. 10, no. 10, pp. 1415-1425, Oct. 1992.

27. G. El-Howayek et al., "On the use of gaussian approximation in analyzing the performance of optical receivers", *IEEE Photon. J.*, vol. 6, no. 1, pp. 1-8, Feb. 2014.

28. D. Snyder, M. Miller, Random Point Processes in Time and Space, New York, NY, USA:Springer-Verlag, 1991.